XMM-Newton Calibration Technical Note

XMM-SOC-CAL-TN-0018

EPIC Status of Calibration and Data Analysis

Edited by M.J.S. Smith (ESAC)
on behalf of the EPIC Consortium

June 29, 2022

History

Version	Date	Editor	Note
3.13	June 29, 2022	Michael Smith	Aligned to SASv20.0; Sects. 6, 10.1 and 11.1; Figs. 8, 10, 11 and 14
3.12	October 23, 2019	Michael Smith	Aligned to SASv18.0; Sects. 6 and 8; Figs. 8, 10, 11 and 14
3.11	July 4, 2018	Michael Smith	Aligned to SASv17.0
3.10	June 28, 2018	Michael Smith	Figs. 1, 10 and 11; Sect. 11 (recommended energy ranges)
3.9	January 2, 2017	Michael Smith	Updated URL
3.8	December 12, 2016	Michael Smith	Aligned to SASv15.0 and SASv16.0; updated URLs
3.7	September 10, 2015	Michael Smith	Aligned to SASv14.0
3.6	September 1, 2014	Matteo Guainazzi	Revision by the XMM-Newton Project Scientist
3.5	August 8, 2014	Matteo Guainazzi	Revision by the XMM-Newton Science Support Manager
3.4	August 8, 2014	Matteo Guainazzi	Aligned to SASv13.5 Fig. 1 (`ELLBETA` calibration accuracy) Fig. 2 (Relative area calibration accuracy)
3.3	October 2, 2013	Matteo Guainazzi	Sect. 6 aligned to XMM-CCF-REL-300 Possible contamination in the MOS cameras (Sect. 2.3)
3.2	August 25, 2013	Matteo Guainazzi	Aligned to SASv13 (see Sect. 12 for a list of changes)
3.1	July 24, 2012	Matteo Guainazzi	Aligned to SASv12
3.0	November 16, 2011	Matteo Guainazzi	First LATEX version (from Version 2.13)

Contents

1 Scope **4**

2 Calibration Overview **4**
2.1 Summary . . . 4
2.2 Summary of Important Improvements Since the Previous Issue . . . 4
2.3 Summary of Important Ongoing Calibration Topics . . . 5

3 Imaging **6**
3.1 Astrometry . . . 6
3.2 Point Spread Function and Encircled Energy . . . 7

4 Effective Area **9**
4.1 Mirror Collecting Area . . . 9
4.2 Filter Transmission . . . 10
4.3 CCD Quantum Efficiency . . . 10
4.4 EPIC-MOS Contamination . . . 12
4.5 Vignetting . . . 12

5 Energy Redistribution **13**
5.1 EPIC-MOS . . . 13
5.2 EPIC-pn . . . 14

6 CTI and Gain **15**

7 Background **18**

8 Timing **20**

9 Cross Calibration **23**

10 Unexpected Events **23**
10.1 Micrometeoroid Impacts . . . 23

11 Data Analysis **24**
11.1 New Features in SAS . . . 24
11.1.1 SASv20.0 . . . 25
11.1.2 SASv19.0 . . . 25
11.1.3 SASv18.0 . . . 25
11.1.4 SASv17.0 . . . 25
11.1.5 SASv16.0 . . . 26
11.1.6 SASv15.0 . . . 26
11.1.7 SASv14.0 . . . 26
11.1.8 SASv13.5 . . . 27
11.1.9 SASv13.0 . . . 27
11.1.10 SASv12.0 . . . 27
11.1.11 SASv11.0 . . . 27
11.1.12 SASv10.0 . . . 27
11.1.13 SASv9.0 . . . 27

11.1.14 SASv8.0 28
11.1.15 SASv7.1 28
11.1.16 SASv7.0 28
11.1.17 SASv6.5 28
11.2 Data Analysis 29
11.2.1 EPIC-MOS 29
11.2.2 EPIC-pn 30
11.2.3 Counting Mode 32

12 History of This Document **32**

1 Scope

This document reflects the status of the calibration of the EPIC camera as implemented in SASv18.0 with the set of calibration files (Current Calibration Files, CCFs) available at the date of the document, unless otherwise specified. Furthermore, the outlook is considered for improvements of calibration, which at the moment can be expected for the next SAS release.

2 Calibration Overview

This section gives a short overview of the status of the calibration of the EPIC instruments MOS1, MOS2 and pn, operating on-board the XMM-Newton observatory. It summarises the quality of the calibration to the extent that this may influence the scientific interpretation of the results. The instrument calibration is based on a combination of physical and empirical models of the various components including mirror response, filter transmission and detector response (energy redistribution, charge transfer efficiency (CTE), gain). During ground calibration various components were calibrated and the model for each component was optimised. These models were verified in flight and are, where relevant, continuously monitored (e.g. contamination of the detector, changes in gain and CTE due to effects of radiation). Corrections, which are needed for these time-variable changes, will be applied to the Current Calibration Files and/or the processing software. For more detailed information see the release notes of the CCFs at: `https://www.cosmos.esa.int/web/xmm-newton/ccf-release-notes`. A general description of the instruments, as well as preliminary calibration results, were published by Turner et al. (2001, A&A, 365. L27; EPIC-MOS) and Strüder et al. (2001, A&A, 365, 18; EPIC-pn).

2.1 Summary

Tab. 1 shows a summary of the status of the calibration for sources at the nominal boresight position ("on-axis").

2.2 Summary of Important Improvements Since the Previous Issue

- **EPIC on-axis flux cross-calibration**: Two empirical corrections to the EPIC effective areas have been released:
  - An update to the existing EPIC-MOS effective area corrections (CORRAREA), derived from analysis of a large sample of on-axis point sources. These corrections empirically reduce spectral differences of the EPIC-MOSs with respect to EPIC-pn above 2 keV and consist of changes to the EPIC-MOS effective areas of up to $\sim 15\%$ at 10 keV.[1]
  - A correction to the EPIC effective areas in order to obtain a better agreement of EPIC-pn with NuSTAR FPMA and FPMB. The changes, which are identical for the three EPIC

[1] `https://xmmweb.esac.esa.int/docs/documents/CAL-SRN-0382-1-1.pdf`

Table 1: Synopsis of the EPIC calibration status

Effect	Maximum Error	Dependency on	
		Energy	Off-Axis Angle
Relative Astrometry	1.5" (1σ)	NO	YES
Absolute Astrometry	1.2" (1σ)	NO	YES
Point Spread Function (PSF)[1]	2%	YES	YES
Relative Effective Area	±3% / 2% (MOS/pn)	YES	YES
Absolute Effective Area	±10%[2]	YES	YES
Absolute Energy Scale	±10 / 12.5 eV (MOS/pn)[3]	YES	YES
Relative Timing	$\Delta P/P < 10^{-8}$	NO	NO
Absolute Timing	$< 70\mu s$	NO	NO

[1]This number represents the maximum inaccuracy of the Encircled Energy Fraction for typical source extraction radii.
[2]In this context, users may refer to the papers written by the International Consortium for High Energy Calibration (IACHEC), available at: `http://web.mit.edu/iachec/papers/index.html`. In particular: Nevalainen et al. (2010, A&A, 523, 22), Tsujimoto et al. (2011, A&A, 525, 25), Ishida et al. (2011, PASJ, 63, 657), Kettula et al. (2013, A&A, 552, 47) and Schellenberger et al. (2015, A&A 575, 30).
[3]±20 eV in EPIC-pn fast modes (Burst and Timing).

cameras, consist of corrections of up to 8% in the 3–12 keV band to reduce differences in spectral shape. No attempt, however, is made to correct the overall relative spectral normalization of EPIC-pn with respect to NuSTAR (EPIC-pn cross-calibration constant of 0.81 ± 0.03 in the 3–12 keV band).[2]

In order to apply either or both of these corrections, they need to be explicitely invoked by the user in the SAS data processing (details may be found in the cited documents; see also Sect. 11.1.1).

- **EPIC-pn Burst Mode energy scale**: Calibration and implementation of the Rate-Dependent PHA correction for EPIC-pn Burst Mode. This empirical correction addresses a rate-dependency of the energy reconstruction seen in high count rate sources observed in EPIC-pn Timing and Burst Modes - for the former, a similar correction had already been implemented[3] whereas the Burst Mode correction was released in June 2020.[4]

- **EPIC-pn energy scale**: The use of the Cu-K_α fluorescence line (at ~ 8.0 keV) as additional calibration point for deriving the long-term CTI (LTCTI) correction for EPIC-pn Full Frame, Extended Full Frame[5] and Large Window mode[4] data.

2.3 Summary of Important Ongoing Calibration Topics

[2]`https://xmmweb.esac.esa.int/docs/documents/CAL-SRN-0388-1-4.pdf`
[3]`https://xmmweb.esac.esa.int/docs/documents/CAL-SRN-0369-0-0.pdf`
[4]`https://xmmweb.esac.esa.int/docs/documents/CAL-SRN-0376-1-1.pdf`
[5]`https://xmmweb.esac.esa.int/docs/documents/CAL-SRN-0389-1-2.pdf`

- **EPIC vignetting**: Radial and azimuthal dependence of EPIC-MOS to EPIC-pn flux ratios have been reported based on large samples of XMM catalogue data (e.g. Mateos et al. 2009, A&A 496 and Lusso 2019, Astron. Nachr. 340, 4). In particular, increased EPIC-MOS w.r.t. EPIC-pn fluxes were seen towards larger off-axis angles (of up to 20% at $\sim 12'$ radial distance). Investigations into the vignetting calibration are ongoing.
- **EPIC response**: Residual inaccuracies in both EPIC-MOS and EPIC-pn responses, especially in the shape of the redistribution function below ~ 2 keV, are being investigated.
- **EPIC-MOS energy scale**: The EPIC energy scale calibration is strongly time dependent mainly due to a steady increase in charge transfer inefficiency (CTI). For EPIC-MOS, the long-term CTI calibration is mainly based on Al-K_α and Mn-K_α lines produced by the on-board ^{55}Fe calibration source. Due to its natural decay, in recent epochs it has become increasingly difficult to obtain accurate CTI measurements. Alternative methods and observations to maintain an acceptable energy scale calibration are being investigated.
- **EPIC-pn energy scale**: A refinement of the EPIC-pn energy scale calibration, improving both temporal and spatial energy reconstruction above ~ 6 keV is being implemented. The method is based on that described in Sanders et al. 2020, A&A, 633, A42.

3 Imaging

3.1 Astrometry

Astrometry: The precision with which astronomical coordinates can be assigned to source images in the EPIC focal plane. We distinguish between: absolute astrometry (precision relative to optical coordinates), relative astrometry within a camera (precision within one camera after correction for systematic offsets due to spacecraft mis-pointing) and relative astrometry between cameras (positions in one camera relative to another).

The XMM-Newton absolute astrometric accuracy is limited by the precision of the Attitude Measurement System. A comparison between the positions measured by the EPIC cameras with respect to the 2MASS reference frame projected onto the spacecraft axis suggested an average 0" shift with a standard deviation $\leq$0.8" per axis (Altieri, 2004, XMM-CCF-REL-168[6]).

Later work has unveiled several issues affecting the accuracy of the EPIC astrometry:

1. A wrong centroiding in detector coordinates of the `MEDIUM` PSF, *i.e.* the default model used for source detection before SASv12. The dynamical range of this effect is $\pm$1", erratically dependent on energy and camera. The `ELLBETA` PSF is not affected by this error. Using the state-of-the-art PSF model cures this issue.
2. A bug in the SAS task `emldetect`, introducing a $\sim 0.7''$ error in the coordinates determination. This bug was fixed with SASv12.

[6] `https://xmmweb.esac.esa.int/docs/documents/CAL-SRN-0168-1-3.ps.gz`

3. Due to an error in a formula within the SAS task `attcalc`, the Euler ψ angle contained in the boresight CCF had the wrong sign. In most cases the two errors would cancel out with no detrimental effect on the SAS astrometry reconstruction. Some tasks, however, used the incorrect boresight values directly, which resulted in a wrong conversion between celestial and detector coordinate systems. The scientific impact is limited to very specific cases which are described in Saxton, 2016, XMM-CCF-REL-332[7]. This issue was corrected in SASv15 (in conjunction with XMM_BORESIGHT_0026.CCF).

Furthermore, it has been shown that the Star Tracker and instrument axes alignments exhibit seasonal dependencies of unknown origin. While their exact pattern depends on the camera and the coordinate system, they can be broadly characterised as a seasonal pattern superimposed on a longer term trend. Similar behaviour is seen when correlating the misalignment against other quantities with a seasonal dependence (such as the astronomical position angle, or the source R.A.). Attempts at correlating the EPIC mis-alignments with housekeeping parameters monitoring the thermal state of the optics have yielded only inconclusive results so far.

The time dependency of the mis-alignments has been empirically modelled by means of a long term variation plus a periodic (nearly one year) oscillation. This constitutes the so-called *time-dependent boresight concept* (Talavera et al. 2012, XMM-CCF-REL-285[8]). The mis-alignments, sampled in five-day intervals, are converted to increments of the Φ and Θ Euler angles. The most recent update of model parameters was in 2018 (Rosen et al. 2018, XMM-CCF-REL-361[9]). The average distribution of the positional offsets between the X-ray and optical source coordinates is centred around 0 along both the Y and the Z spacecraft coordinates. The width of the offset distributions is $\simeq 1.2''$.

3.2 Point Spread Function and Encircled Energy

Point Spread Function: The spatial distribution of light in the focal plane in response to an observed (monochromatic) point source. The PSF integrates to 1 over the infinite focal plane. Encircled Energy: The fraction of the energy of a point source collected within a certain radius.

With SASv10, a full 2-D parametrisation of the EPIC PSF as a function of instrument, energy and off-axis angle covering the whole field-of-view was introduced. A full description is available in Read et al. (2011, A&A, 534, 34).

This model is the default as of SASv12, and superseded all previously existing models both for source detection as well as for the calculation of the Encircled Energy Fraction by `arfgen` (Read & Saxton, 2012, XMM-CCF-REL-280[10]). It is a semi-analytical model of stacked images of sources from the 2XMM Serendipitous Catalogue (Watson et al. 2009, A&A, 493, 339). It models the PSF spokes and the large-scale azimuthal variations, and includes an additional Gaussian core (which accounts for (at most) 2% of the enclosed energy flux in the EPIC-MOS cameras). The production

[7] `https://xmmweb.esac.esa.int/docs/documents/CAL-SRN-0332-1-0.ps.gz`
[8] `https://xmmweb.esac.esa.int/docs/documents/CAL-SRN-0285-1-0.ps.gz`
[9] `https://xmmweb.esac.esa.int/docs/documents/CAL-SRN-0361-1-0.pdf`
[10] `https://xmmweb.esac.esa.int/docs/documents/CAL-SRN-0280-1-2.ps.gz`

of the EPIC Serendipitous Source Catalogue (a.k.a. the "3XMM Catalogue") was based on this PSF model.

The parameters describing the PSF shape were refined in a 2017 calibration release in order to address significant spectral discrepancies between PSF core and wings. In addition, the PSF normalisation radius was modified in order to correct overestimates of the telescope effective area (Smith et al. 2017, XMM-CCF-REL-348[11]). The overall accuracy of the model with respect to the integrated PSF is within 3% (Fig. 1).

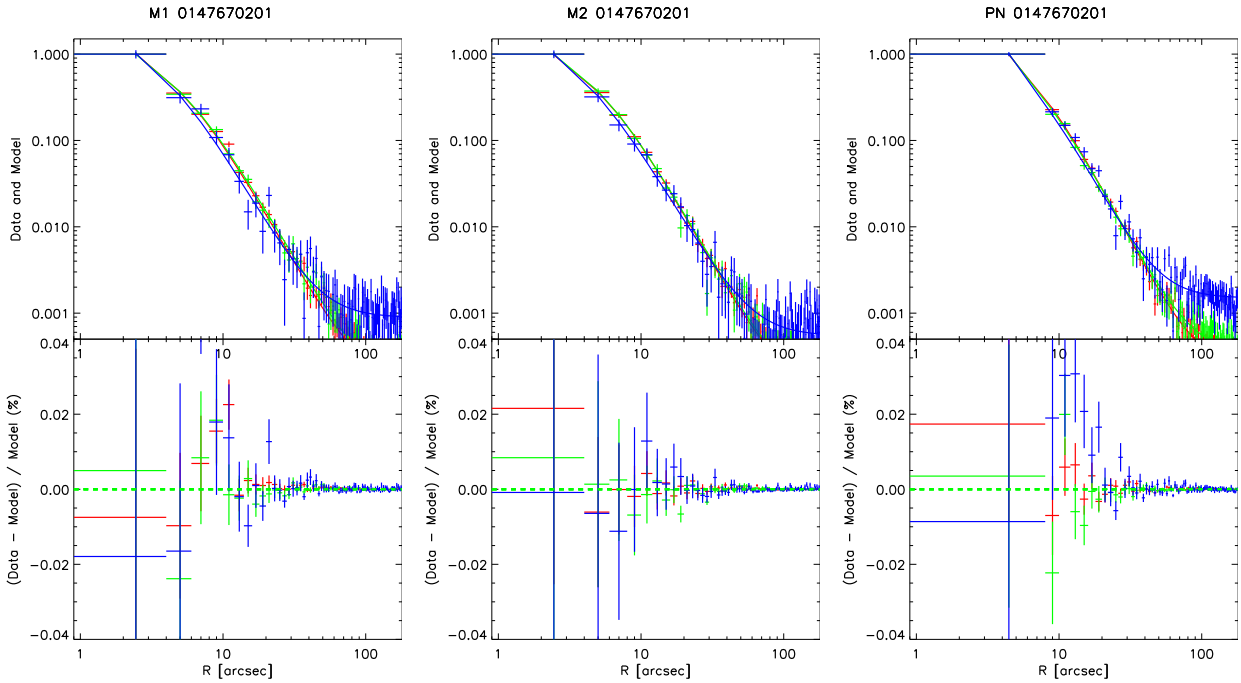

Figure 1: *Upper panels*: Normalised `ELLBETA` PSF profiles (*dashed lines*) compared against the measured radial profiles of the QSO PKS B1334-127 (Obs. 0147670201) in three energy bands: 1–2 keV (*red*); 2–4.5 keV (*green*); 4.5–10 keV (*blue*). *Lower panels*: percent residuals between the observed and modelled PSF radial profiles. *Left panels*: EPIC-MOS1; *centre panels*: EPIC-MOS2; *right panels*: EPIC-pn

[11] `https://xmmweb.esac.esa.int/docs/documents/CAL-SRN-0348-1-1.pdf`

4 Effective Area

Effective Area: the collecting area of the optical elements folded with the energy-dependent sensitivity of the detector systems of the EPIC cameras.

The internal accuracy in the determination of the total effective area over the spectral range from 0.4–12 keV is better than 3% and 2% (at 1-σ) for the EPIC-MOS and EPIC-pn cameras respectively (see Fig. 2).

The cross calibration between EPIC-MOS1 and EPIC-MOS2 agrees within 4%. The MOS/pn global flux normalisation agrees to 8% from 0.4 keV to 12 keV. A statistical assessment of the relative flux cross-calibration among the X-ray cameras on board XMM-Newton is discussed in Stuhlinger et al. (2010, XMM-SOC-CAL-TN-0052[12]) and Read et al. (2014, A&A, 564, 75).

As of SASv14.0, a non-default option allows an empirically derived correction to be applied to the EPIC effective areas (Guainazzi et al. 2014, XMM-CCF-REL-321[13]). This `CORRAREA` correction can be used to evaluate the impact of the current relative uncertainties in the effective area calibration on parameters derived from spectral fitting. Although this allows to estimate the effect of these systematic errors, it is emphasised that, pending further validation, this correction is *not* meant to be used as a replacement of the nominal calibration. The `CORRAREA` correction can be invoked through the `applyxcaladjusment` option in the `arfgen` task.

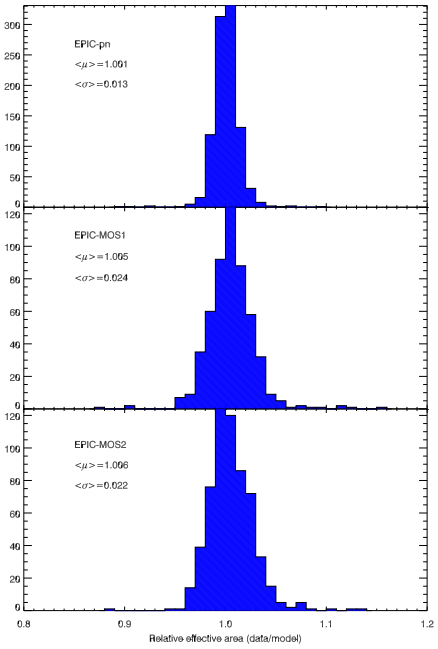

Figure 2: Distribution of residuals against the best-fit logarithmic power-law model on a sample of 90 observations of radio-loud AGN extracted from the XMM-Newton cross-calibration database (Stuhlinger et al. 2010, XMM-SOC-CAL-TN-0052)

4.1 Mirror Collecting Area

Mirror collecting area: the face-on area of the mirror system that reflects X-rays to the focal region.

The mirror collecting area has been measured on ground and verified in orbit. However, XMM-Newton EPIC-pn observations with very high statistics still showed residuals above 6 keV. This was addressed in a mirror effective area calibration update released in 2006[14].

[12] `https://xmmweb.esac.esa.int/docs/documents/CAL-TN-0052.ps.gz`
[13] `https://xmmweb.esac.esa.int/docs/documents/CAL-SRN-0321-1-2.ps.gz`
[14] `https://xmmweb.esac.esa.int/docs/documents/CAL-SRN-0205-1-0.ps.gz`

4.2 Filter Transmission

Filter transmission: the fraction of incident X-ray photons that pass through the filter.

The filter transmission has been measured on ground. Fig. 3 shows filter transmission curves for all the cameras. For the thick filter the green curve shows the single transmission function currently used in the CCFs for MOS1, MOS2 and pn.

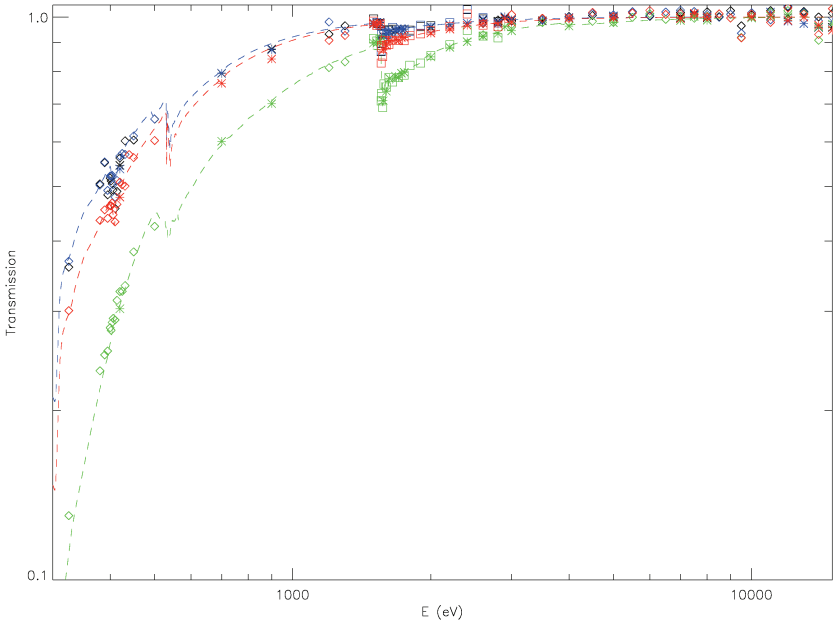

Figure 3: Filter transmission in CCF and in ground calibration filter measurement data points. *Green*: THICK; *red*: MEDIUM; *blue*: THIN. Ground measurements are labelled with *symbols*: *stars*: EPIC-MOS1; *diamonds*: EPIC-MOS2; *squares*: EPIC-pn. The CCF values are indicated by the *dashed lines*.

In Autumn 2012 a specific calibration experiment was performed on the thermal SNR 1E 0102-7219 to test in-flight the accuracy in the calibration of the filter transmission. The results are summarised in Fig. 4. For all cameras and all filters, the residuals against the same astrophysical model (Plucinsky et al. 2012, SPIE, 8443, 12) with the same parameters tied together are consistent within statistics (*i.e.* within ±1%).

4.3 CCD Quantum Efficiency

Quantum Efficiency (QE): the fraction of incident photons on the detector that generate an event in the CCD.

Recalibration of the EPIC-MOS QE (Sembay, 2007, XMM-CCF-REL-235[15]) in 2007 led to an increase of the surface layers of C, N and O (see Fig. 5). Nitrogen and Oxygen are constituents of

[15] `https://xmmweb.esac.esa.int/docs/documents/CAL-SRN-0235-1-0.ps.gz`

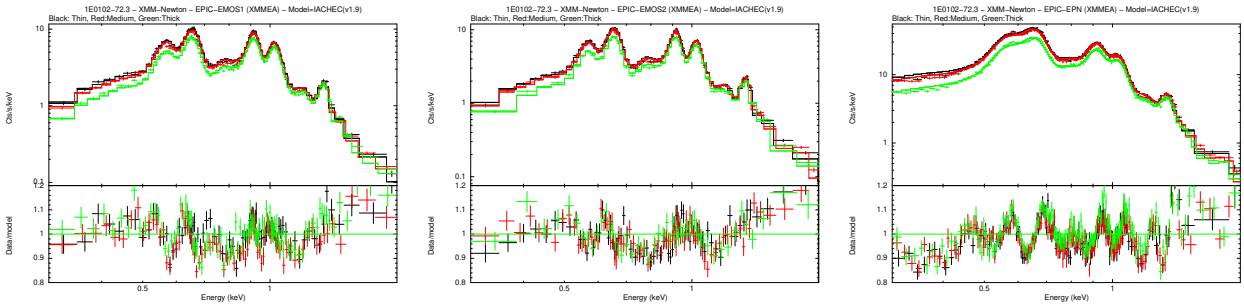

Figure 4: *Upper panels*: spectra of the thermal SNR 1E 0102-7219 observed with different optical blocking filters in Rev. 2380: *black* = `THIN`; *red* = `MEDIUM`; *green* = `THICK`. *Lower panels*: residuals against the same astrophysical model (based on the IACHEC study after Plucinsky et al. 2012; details in text). *Right panel*: EPIC-MOS1; *centre panel*: EPIC-MOS2; *left panel*: EPIC-pn.

the surface layers of the CCDs and the level of increase of these depths is within the accuracy of physical measurements of the CCD structure. Carbon is not a natural layer on the CCD. It has been added to the QE model primarily because an additional edge at this energy is most compatible with the existing redistribution function.

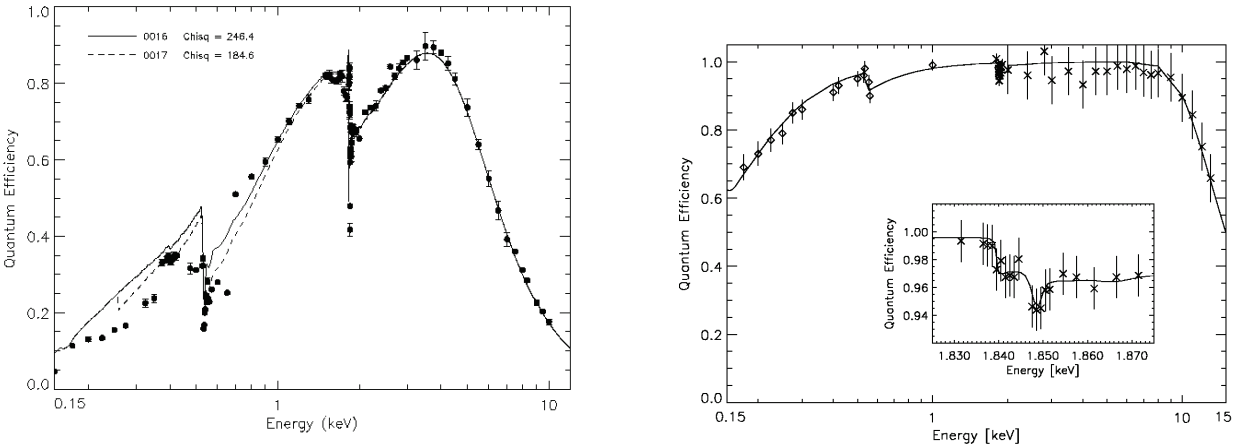

Figure 5: *Left panel*, EPIC-MOS QE ground calibration measurements (*data points*), pre-2007 QE model (*solid line*), post-2007 QE model (*dashed line*). Right panel: EPIC-pn QE ground measurements (*data points*) and model (*solid line*).

Ground calibration measurements have shown that the quantum efficiency of EPIC-MOS CCDs is spatially uniform above 400 eV (see Fig. 6).

Below this energy spatial variations within a CCD are seen as patches in the outer parts of the CCDs where the response is degraded. This inhomogeneity is currently not taken into account by the SAS.

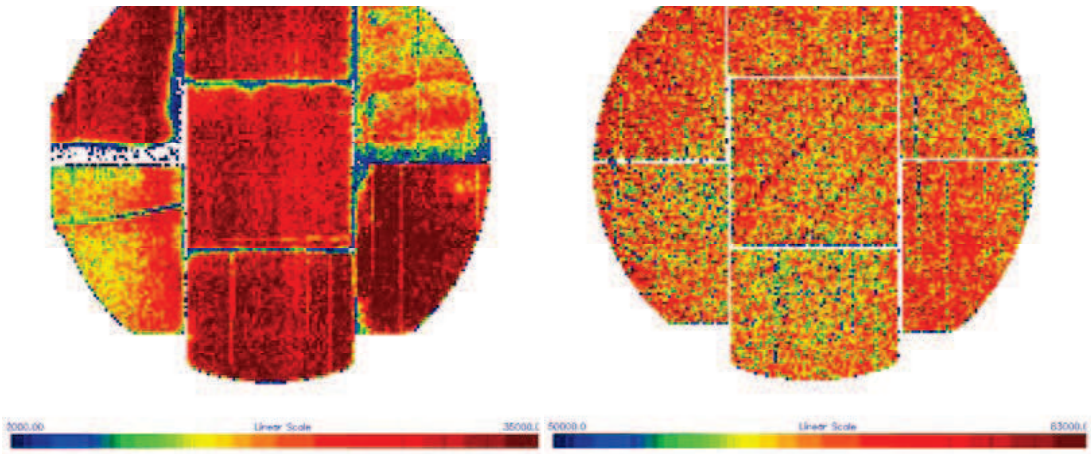

Figure 6: QE spatial inhomogeneities, appearing only at very low energies (*left panel*: 150 eV; *right panel*: 400 eV). The *colour bars* correspond to a factor 17 and 1.3, respectively.

4.4 EPIC-MOS Contamination

It has become apparent that the response of the EPIC-MOS cameras (primarily MOS2) has deteriorated at low-energies ($\leq$1 keV) over the course of the mission. It is suspected that this is due to contaminants which have adhered to the surface of the cameras, absorbing a fraction of the incoming photons. A calibration of the time evolution of this contaminant has been publicly available as of SASv13.5 (Sembay & Saxton, 2013, XMM-CCF-REL-305[16]). The EPIC-MOS contaminant is currently modelled as pure Carbon, similar to that observed on the RGS.

4.5 Vignetting

Vignetting: reduction in the effective area with radial distance from the telescope's axis.

The telescope vignetting is well determined for off-axis angles of up to more than 10'. Fig. 7 shows the average vignetting measured over 4 azimuths at an off-axis angle of around 10' derived from calibration measurements of the SNR G21.5-09. With the latest calibration of the position of the telescope axis (embedded in `XMM_MISCDATA_0020`), the differences in flux for off axis sources for each camera are $\simeq$5%. Detailed information can be found in Lumb et al. (2004, astro-ph/0403647) and Read (2004, XMM-CCF-REL-167[17]). However, larger differences among the EPIC cameras have been unveiled by a study of a large sample of 2XMM serendipitous sources (Mateos et al. 2009, A&A, 496, 879). Investigation into the causes of these discrepancies is ongoing.

[16] `https://xmmweb.esac.esa.int/docs/documents/CAL-SRN-0305-1-0.ps.gz`
[17] `https://xmmweb.esac.esa.int/docs/documents/CAL-SRN-0167-1-1.ps.gz`

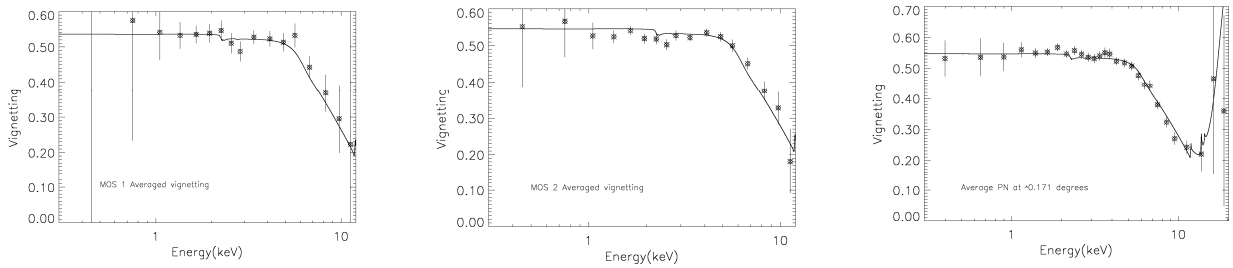

Figure 7: Average vignetting measured over 4 azimuths at an off-axis angle of around 10' derived from the calibration measurements of G21.5-0.9

5 Energy Redistribution

Energy Redistribution: The energy profile recorded by the detector system in response to a monochromatic input. This includes the spreading of the recorded energy due to the statistical nature of charge collection (i.e. the energy resolution) and also charge loss effects, which distort the profile.

The energy resolution is monitored by the on-board calibration source, which produces strong Al-K$_\alpha$ (1.487 keV) and Mn-K$_\alpha$ (5.893 keV) emission lines. The resolution of the EPIC-MOS cameras degraded significantly with time up to the epoch where the cameras were cooled (Fig. 8). After this epoch the degradation in energy resolution has been small. For the EPIC-pn camera, the line width at Mn-K$_\alpha$ increases by $\simeq$2.5 eV/year. As of SASv14.0 this decrease in resolution is taken into account through a time-dependent response function.

Pre-calculated ("canned") redistribution matrices for most instrumental configurations, and a range of source positions and observation epochs are available at:
`https://www.cosmos.esa.int/web/xmm-newton/epic-response-files`.

5.1 EPIC-MOS

The low energy redistribution function (RMF) of the EPIC-MOS CCDs has a complex shape, in that the main photo peak has a secondary component (a shoulder) which relatively increases with decreasing energy, until, at the very lowest energies, it is the dominant component. Observations of non- or weakly-varying sources, such as the SNR 1E 0102-7219 and the O-star ζ Puppis, have shown that the shape of the in-flight redistribution function changes both spatially across the detector (the change from the on-ground calibration being most pronounced at the boresight) and also evolves with observation epoch (Read et al. 2005, ESA-SP 604). The form of this was such that the original shoulder evolved into a flatter 'shelf', of lower amplitude, but extending to lower energies. The bulk of the spatial change occurs within 40 arc-seconds of the boresight, a region which we refer to as the "patch". A new method of deriving the RMF was incorporated in SASv11.0. There are three RMF regions on each of the two EPIC-MOS detectors; a "patch core" region, a "patch wings" region and an "outside patch" region (see Fig. 9). This, in combination with the 13 temporal epochs now considered in the SAS, two types of `PATTERN` selection (single events and standard `PATTERN<13`) and two cameras gives rise to a total of 156 EPIC-MOS RMFs in the current calibration files. For a source extracted close to the patch (e.g., as in figure with patch), `rmfgen` automatically constructs

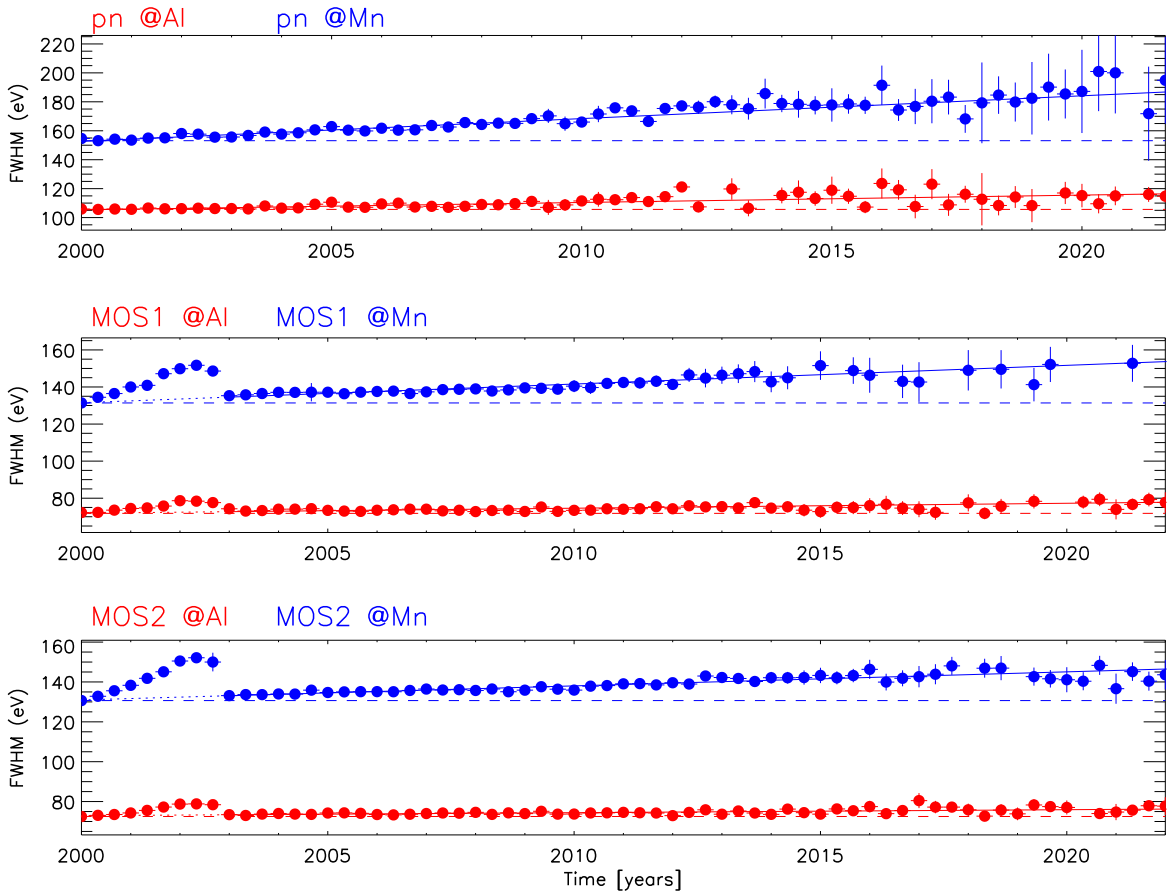

Figure 8: Energy resolution in the EPIC-pn CCD4 (top), EPIC-MOS1 CCD1 (middle), and EPIC-MOS2 CCD1 (bottom). Colours code different lines emitted by the calibration source.

a PSF-(default) or flat-weighted average RMF from the three region-defined RMFs (making use, of course, of the calibration files from the correct epoch). Users are referred to the CCF Release Note (Sembay et al. 2011, XMM-CCF-REL-272[18]).

5.2 EPIC-pn

The physical parameters describing the EPIC-pn redistribution were calibrated using a suite of line-rich and continuum astrophysical sources. Empirical models of the RGS spectra were used to describe the former. The response matrices are dependent on readout mode, although per mode they are identical for all CCDs (note that for SW, TIMING and BURST modes only the CCD containing the focal point is used); the only spatial dependence of the redistribution (i.e. the energy resolution) is in RAWY (see 2.2.2). Other off-axis (radial) dependencies do not exist in the redistribution; specifically, vignetting is an effective area component, computed by `arfgen`.

Measurements of the on-board calibration source at Mn-K_α show a degradation of the energy

[18] `https://xmmweb.esac.esa.int/docs/documents/CAL-SRN-0272-1-0.ps.gz`

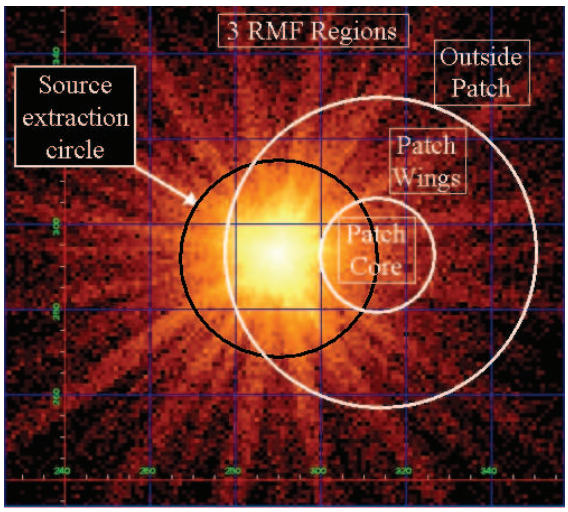

Figure 9: Scheme of the so-called "MOS redistribution patch" (details in text)

resolution of about 2.5 eV/year for Full Frame mode data at the boresight location. This trend is confirmed by measurements of the Fe-K emission of the Circinus Galaxy from observations taken in 2001 and 2014. As of SASv14.0 this is taken into account through the creation of time-dependent response matrices (Saxton et al. 2014, XMM-CCF-REL-322[19]).

The stability and overall performances of the redistribution in the softest X-ray band are regularly monitored through observations of the isolated neutron star RX J1856.6-3754. The spectra taken at different epochs, and their residuals against the baseline model as described in Burwitz et al. (A&A, 2001, 379, L35) are stable. The stability is quantified to be better than 3% (3σ) (Sartore et al. 2012, A&A, 541, 66). The average column density ($\langle N_H \rangle$=6×10^{19} cm^{-2}, σ_{N_H}=6×10^{18} cm^{-2}) is comparable to that measured in a deep (500 ks) LETG high-resolution spectrum ($\langle N_H \rangle$=6×10^{19} cm^{-2}).

6 CTI and Gain

CTI: Charge Transfer Inefficiency is the imperfect transfer of charge as it is transported through the CCD to the output amplifiers during read-out. Gain: Gain is the conversion (amplification) of the charge signal deposited by a detected photon from ADU (Analogue to digital unit) charge into energy (electron-volts).

For the instruments in normal conditions, the Gain and CTI are currently known to the extent that the line energy can be determined with an uncertainty of 5 eV over the full energy range for all EPIC-MOS imaging modes and with an uncertainty of 12 eV over the full energy range for all EPIC-pn imaging modes. The relative accuracy of the Timing modes compared to the imaging modes is better than 1% over the full energy range (see Guainazzi et al. 2011, XMM-SOC-CAL-TN-0083[20]; and Guainazzi, 2010, XMM-SOC-CAL-TN-0082[21]).

[19] https://xmmweb.esac.esa.int/docs/documents/CAL-SRN-0322-1-0.ps.gz
[20] https://xmmweb.esac.esa.int/docs/documents/CAL-TN-0083.pdf
[21] https://xmmweb.esac.esa.int/docs/documents/CAL-TN-0082.pdf

The situation is different for abnormal conditions at the time of strong solar flares or during eclipse seasons. In the latter case, the early part of the revolution may be subject to temperature deviations of the on-board electronics which result in variations in the detector gain. For the EPIC-pn, this is addressed through a temperature dependent gain correction (Kirsch et al. 2007, XMM-CCF-REL-223[22]) which was implemented as default as of SASv7.1.2. For the EPIC-MOS, no such correction has been yet been derived. However, the effect of the EMAE (EPIC-MOS Analogue Electronics) temperature excursions during scientific observations are usually small (MOS1:<10 eV at Mn-K and <5 eV at Al-K).

The accuracy of the energy reconstruction in imaging modes is mainly limited by the accuracy of the time-dependency correction to the gain and CTI. Regular updates of this "long-term CTI" correction are performed, based on the analysis of the calibration source spectra. For EPIC-pn, an additional systematic energy shift can be introduced in the estimate of the zero-energy level. This is determined at the start of the exposure through the so-called offset map, which is calculated in instrumental energy bins of 5 eV. In spectral analysis, these effects can be corrected by allowing a small ($\lesssim$ 10 eV) shift in instrumental gain (e.g. through the `gain fit` command in *XSPEC* or `gainshift` kernel in *ISIS*).

For EPIC-pn, SASv14.0 introduced an energy dependency in the long-term CTI correction. Previously, the modelling was based on the trend at Mn-K$_\alpha$ ($\sim$ 5.9 keV). However, as the rate of increase of CTI is energy dependent, this led to an increasing energy overcorrection at lower energies. The current calibration includes an additional modelling based on the trend as measured at Al-K$_\alpha$ (Smith et al. 2014, XMM-CCF-REL-323[23]) and, since 2019, also at the Cu-K$_\alpha$ fluorescence emission (Valtchanov et al. 2019, XMM-CCF-REL-367[24], Migliari et al. 2020, XMM-CCF-REL-376[25], Valtchanov et al. 2022, XMM-CCF-REL-389[26]).

The most recent updates of the EPIC-MOS long-term CTI and gain corrections are discussed in Stuhlinger, 2019, XMM-CCF-REL-363[27] and XMM-CCF-REL-364[28]. Extrapolation of the long-term CTI and gain correction model to more recent epochs results in an undercorrection of the EPIC-MOS energy reconstruction (of up to 8 eV at Al-K$_\alpha$ and 15 eV at Mn-K$_\alpha$, depending on the MOS unit and CCD). An update of the model to address these issues is currently being under development.

The calibration line energy reconstruction over the course of the mission is shown in Fig. 10 for EPIC-MOS and Fig. 11 for EPIC-pn.

[22] `https://xmmweb.esac.esa.int/docs/documents/CAL-SRN-0223-1-0.ps.gz`
[23] `https://xmmweb.esac.esa.int/docs/documents/CAL-SRN-0323-1-1.ps.gz`
[24] `https://xmmweb.esac.esa.int/docs/documents/CAL-SRN-0367-1-0.pdf`
[25] `https://xmmweb.esac.esa.int/docs/documents/CAL-SRN-0376-1-1.pdf`
[26] `https://xmmweb.esac.esa.int/docs/documents/CAL-SRN-0389-1-2.pdf`
[27] `https://xmmweb.esac.esa.int/docs/documents/CAL-SRN-0363-1-1.pdf`
[28] `https://xmmweb.esac.esa.int/docs/documents/CAL-SRN-0364-1-0.pdf`

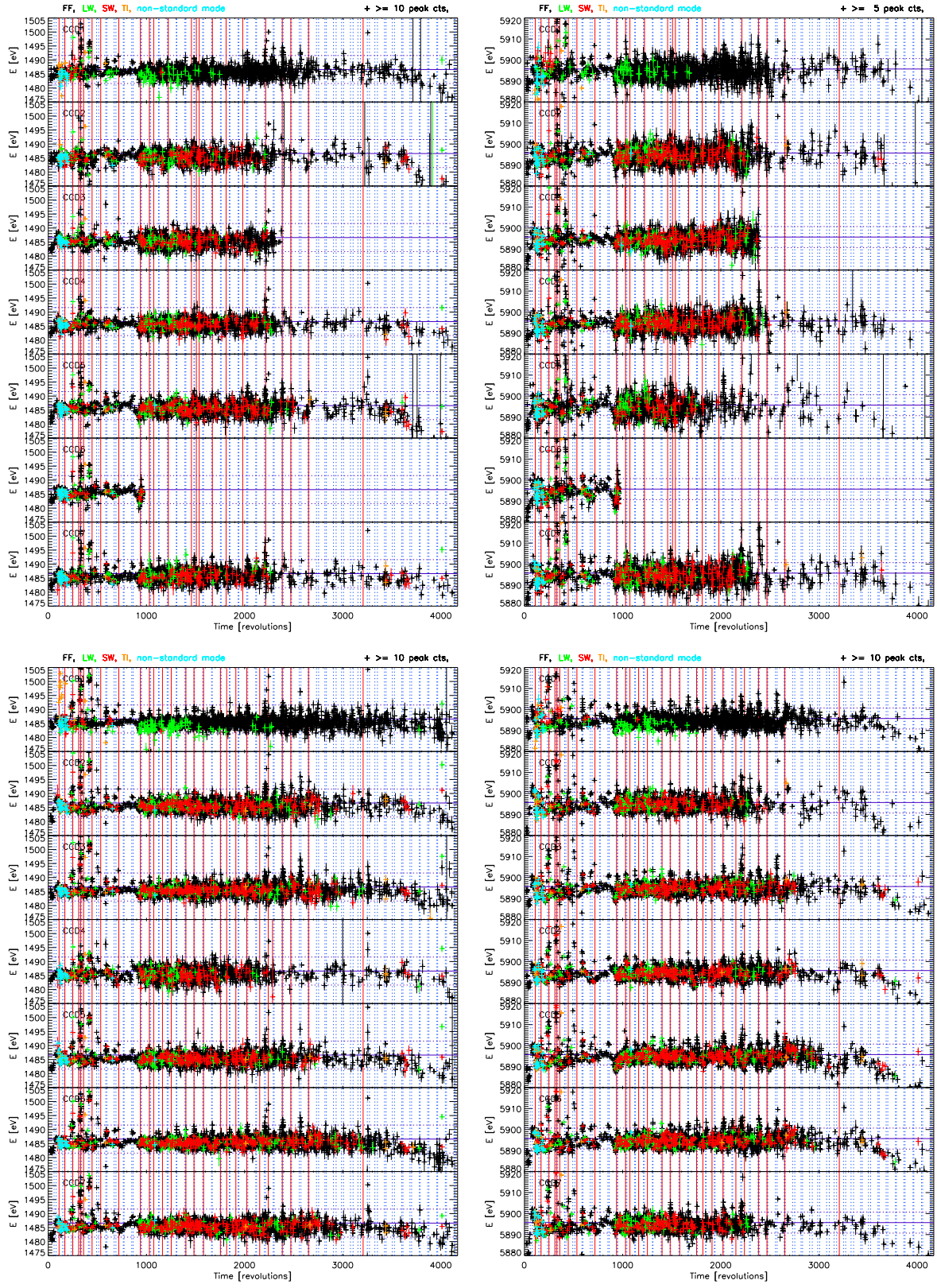

Figure 10: *Top*: EPIC-MOS1 Al-K$_\alpha$ (*left panel*) and Mn-K$_\alpha$ (*right panel*) energy scales for patterns 0–12 after the application of the current long-term CTI and gain corrections. Eclipse seasons are indicated by *vertical blue lines*, CCF epochs by *red lines*. The *horizontal solid lines* represent the laboratory energy, the *dotted lines* the ±5 eV interval. *Bottom*: The same for EPIC-MOS2.

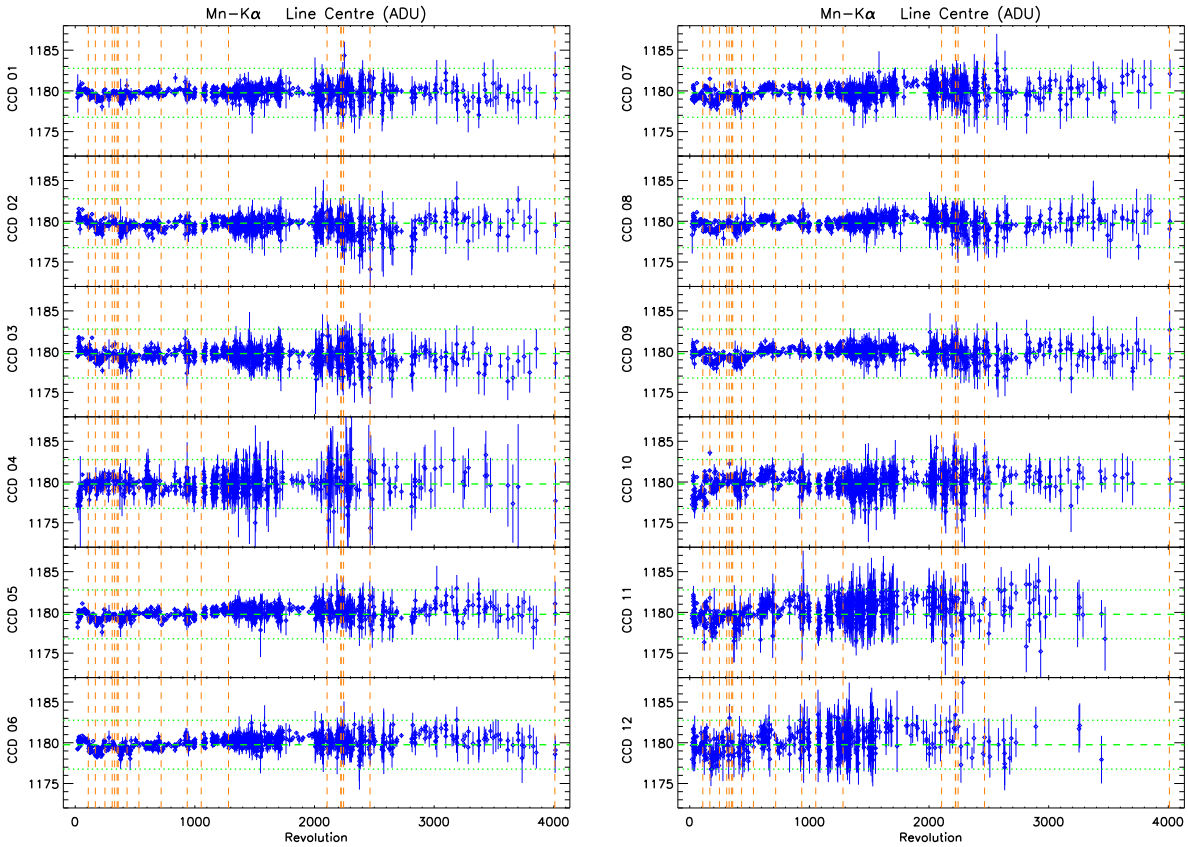

Figure 11: The same as Fig. 10 for EPIC-pn Mn-K$_\alpha$ (values are in ADU). Data from CCD 04 are taken from the 20-row region around the boresight. The *red vertical lines* indicate the times of mayor solar coronal mass ejections. The *green horizontal lines* indicate the nominal laboratory energy (*drawn*), and the ±3 ADU interval (*dashed*).

7 Background

The XMM-Newton observatory provides good capabilities for detecting low surface brightness emission features from extended and diffuse galactic and extragalactic sources, by virtue of the large field of view of the X-ray telescopes and the high throughput yielded by the heavily nested telescope mirrors. In order to exploit the excellent EPIC data from extended objects, the EPIC background, now known to be higher than estimated pre-launch, has to be understood thoroughly.

Detailed information on the treatment of the EPIC background is provided on a dedicated web page at the XMM-Newton SOC portal at:
`https://www.cosmos.esa.int/web/xmm-newton/background` where several dedicated tools and files are available for use in dealing with the EPIC background.

There are several different components to the EPIC background:

1. Photons

- The astrophysical background, dominated by thermal emission at lower energies (E<1 keV) and a power law at higher energies (primarily from unresolved cosmological sources). This background varies over the sky at lower energies.
- Solar wind charge exchange (Carter et al. 2011, A&A, 523, A115).
- Single reflections from outside the field of view, out-of-time events etc.

2. Particles

   - Soft proton flares with spectral variations from flare to flare. This component can be filtered out by selecting quiet time periods from the data stream for analysis. To identify intervals of flaring background the observer should generate a light curve of high energy (E>10 keV) single pixel (`PATTERN`=0) events. To identify good time intervals use the selection criteria:
     - EPIC-MOS: <0.35 cts/s (`#XMMEA_EM && (PI>10000) && (PATTERN==0)` on the full FOV.
     - EPIC-pn: <0.4 cts/s (`#XMMEA_EP && (PI>10000) && (PI<12000) && (PATTERN==0)` on the full FOV.

     These selection criteria assume that sources above 10 keV do not contribute significantly to the overall intensity
   - Internal (cosmic-ray induced) background, created directly by particles penetrating the CCDs and indirectly by the fluorescence of satellite material to which the detectors are exposed.

3. Electronic Noise: Bright pixels and columns, readout noise, etc.

Fig. 12 shows the strong metal line features that make the background subtraction complex, especially for extended sources. In EPIC-pn the background maps vary significantly with energy

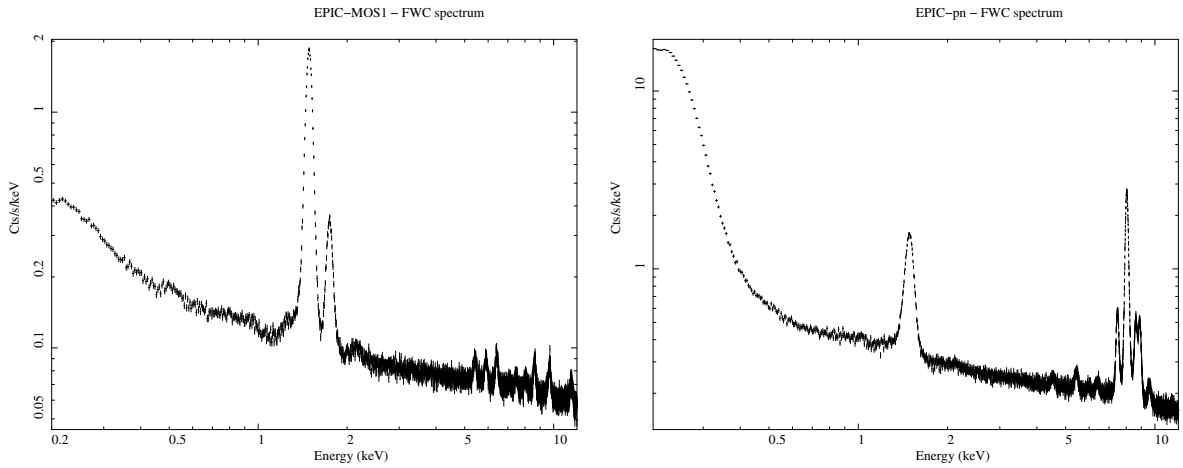

Figure 12: Instrumental background for the EPIC-MOS (*left panel*) and EPIC-pn (*right panel*) in the 0.2–12 keV energy band obtained from exposures taken with the `CLOSED` filter.

energies (Fig. 13). Furthermore, CCD5 in MOS2 (and, at a lower level CCD4 in both MOS cameras) is affected by recurrent, randomly occurring high level of instrumental noise. The origin of this

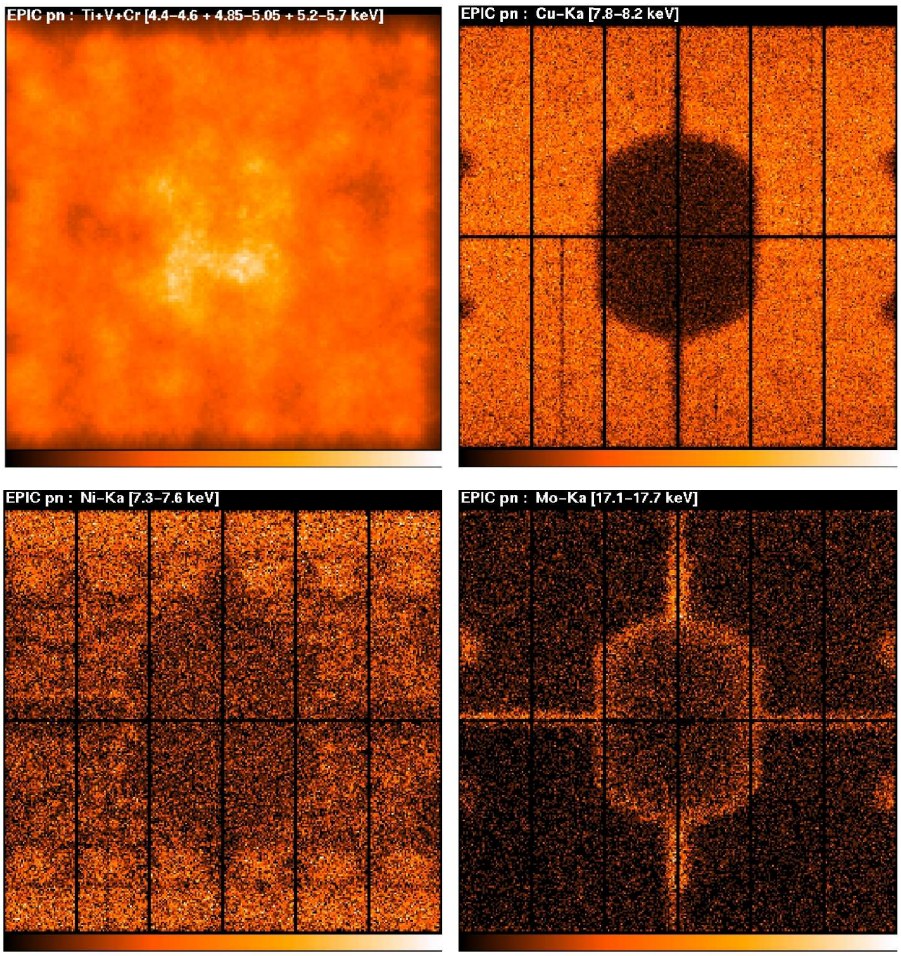

Figure 13: EPIC-pn instrumental background maps at different energies.

feature is still unknown. A SAS task (`emtaglenoise`) has been available as of SASv9.0 to flag noisy frames characterised for subsequent removal.

Readers are referred to Carter & Read (2007, A&A, 464, 1155) for a detailed discussion of the EPIC instrumental background and its components.

8 Timing

Absolute timing: Locating events in time with reference to standard time defined by atomic clocks or other satellites. Relative timing: The capacity to measure time intervals and periodicity reliably.

As of SASv5.3.3 all necessary components have been available to support timing analysis with the nominal time resolutions down to 29 and 7 μs for EPIC-pn Timing and Burst modes, respectively. The accuracy of the EPIC timing is regularly monitored through biannual observation sets of the Crab pulsar. In each observation set EPIC-pn is configured in both Burst and Timing Mode, with

each exposure scheduled at different phases of a single orbit to cover different time delays and ground station data links. Fig. 14 shows the relative and absolute timing accuracy based on the Crab pulsar observations. The relative deviation in the observed pulse period with respect to the most accurate radio data available (ΔP/P) is considerably less than 3×10^{-8} ($1\sigma=1\times10^{-8}$), with an absolute timing accuracy of <70 microseconds (although the Crab observations in revolutions 3435 and 3436 show significantly discrepant values, the cause of which is currently under investigation (Ebrero, 2019, XMM-SOC-CAL-TN-0220[29]).

For the Crab observations, a systematic absolute timing offset between EPIC-pn Timing Mode and Burst Mode has been noted (L. Kuiper, private communication), the origin of which is currently under investigation.

The longer frame times make the EPIC-MOS cameras less suitable for accurate timing studies than the EPIC-pn. Moreover, the accuracy of the timing reconstruction in the EPIC-MOS cameras has not been the subject of sufficient calibration work so far. Users are **urged not to use EPIC-MOS data for timing analysis** whenever high level of accuracy are required.

As part of the SAS data reduction, the conversion from Spacecraft-On-board-Time (OBT) to Mission-Elapsed-Time (MET) can use either the standard real-time Time Correlation (TCS) data, or the Reconstructed Time Correlation (TCX) data, which is the result of a reprocessing designed to eliminate anomalies present in real-time data. The TCX are more precise and the SAS will default to using this data when available in the ODF, which is the case for the vast majority of observations. In some cases, however, the TCX file is not available in the ODF, and the SAS will then automatically use the TCS data. In general the two give similar results, yielding time conversions within $\sim 30\mu s$. However, when no TCX file is present this may point to an anomaly which may have adversely affected the TCS conversions. In such rare cases caution should be exercised when interpreting results.

In November 2009 the regeneration of Time Correlation (TCX) files for all XMM-Newton observations after Rev. 300 was completed. Users are recommended to use the latest ODF (available by default in the XSA) whenever they need the highest possible timing accuracy for the scientific goals of their XMM-Newton data analysis.

An improved algorithm to detect and correct sporadic "jumps" in the flow of the photon arrival times as registered by the EPIC-pn camera was implemented in SASv13.5. It is based on a recalibration of the time evolution of the frame time due to a slow non-linear degradation of the on-board oscillator (Saxton & Freyberg, 2013, XMM-CCF-REL-295[30]). In the event of a EPIC-pn exposure being affected by a time jump (as indicated by the output of `epframes` with `SAS_VERBOSITY`$\geq$5), the user is encouraged to contact the Science Operation Centre helpdesk (`https://www.cosmos.esa.int/web/xmm-newton/xmm-newton-helpdesk`) for advice.

[29] `https://xmmweb.esac.esa.int/docs/documents/CAL-TN-0220-1-2.pdf`
[30] `https://xmmweb.esac.esa.int/docs/documents/CAL-SRN-0298-1-0.ps`

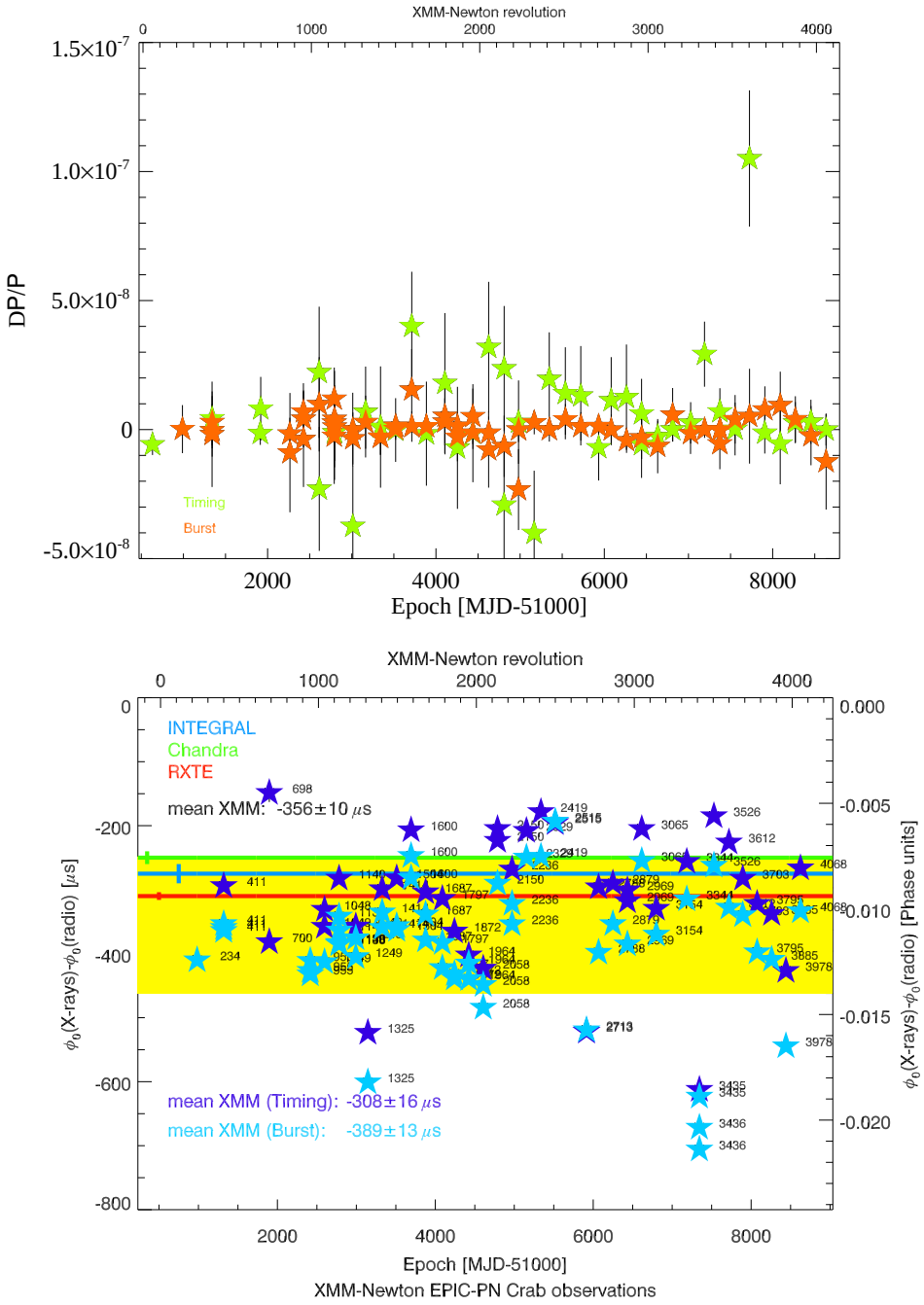

Figure 14: *Top panel*: Relative timing accuracy for the Crab as function of mission time. *Bottom panel:* absolute timing delay measurements of the primary pulses of the Crab pulsar, obtained with EPIC-pn, measured with respect to the Jodrell Bank radio ephemeris. The yellow band indicates the confidence interval of the XMM-Newton measurements in units of $\pm 1\sigma$ (SD) from the mean. The blue, red and green horizontal lines indicate the INTEGRAL, RXTE (Molkov, Jourdain & Roques, 2010, ApJ, 708, 403) and Chandra (see https://cxc.harvard.edu/ccr/proceedings/03 proc/presentations/rots/) measurements, respectively - the small coloured vertical bars in each case indicate their 1σ statistical error. The errors given for the XMM-Newton values are the formal errors on the mean.

9 Cross Calibration

A dedicated Cross-Calibration Document (Stuhlinger et al. 2010, XMM-SOC-CAL-TN-0052[31]) describes the methods and data samples used in determining the cross-calibration status of the XMM-Newton instruments. The results presented in this document were obtained using SASv10 (December 2010). More recent results may be found in e.g. presentations made at the Users' Group meetings (`https://www.cosmos.esa.int/web/xmm-newton/users-group`). The cross-calibration status of the XMM-Newton instruments as of SASv15 (February 2016) can be summarised as follows:

- At energies < 0.54 keV (fluorescent photo-absorption edge of neutral Oxygen) RGS yields fluxes typically 3% larger than those of EPIC-pn.
- At energies > 0.54 keV RGS yields fluxes typically 4% lower than EPIC-pn.
- At energies < 0.85 keV EPIC-MOS and EPIC-pn yield consistent fluxes.
- At energies > 0.85 keV EPIC-MOS yields typically 7% higher fluxes than EPIC-pn.

The EPIC-MOS cameras yield typically mutually consistent fluxes over their whole energy bandpass.

10 Unexpected Events

10.1 Micrometeoroid Impacts

To date, EPIC has suffered six events which have resulted in permanent damage to the detectors. These events, ascribed to micrometeoroid impacts along the boresight, are characterised by a sudden and short optical flash and physical damage to the detectors. In four cases the lasting effect was limited to the appearance of individual bright pixels (Rev. 156 (15 October 2000) in EPIC-pn, Rev. 325 (17 September 2001) in EPIC-MOS1, Rev. 490 (12 August 2002) in EPIC-MOS2 and Rev. 3166 (23 March 2017) in EPIC-MOS2). However two events additionally resulted in more extensive damage: the loss of EPIC-MOS1 CCD6 and the appearance of a hot column passing very close to the EPIC-MOS1 boresight (Rev. 961 on 9 March 2005, see `https://www.cosmos.esa.int/web/xmm-newton/mos1-ccd6`) and the loss of EPIC-MOS1 CCD3 (Rev. 2382 on 11 December 2012, see `https://www.cosmos.esa.int/web/xmm-newton/mos1-ccd3`). In addition, few cases of flash events without associated damage have been detected (e.g. in Revs. 2370 in EPIC-MOS1 and 2468 in EPIC-MOS2).

The events are interpreted as micrometeoroid dust scattered off the mirror surface under grazing incidence and reaching the focal plane detector. The typical particle size is estimated at <1 micron. The origin is most probably interplanetary (or interstellar) dust but not linked to meteor showers, the latter having larger sizes and higher masses (see Abbey et al. ESA proceedings SP-604, Kirsch

[31] `https://xmmweb.esac.esa.int/docs/documents/CAL-TN-0052.ps.gz`

et al. 2005, Proc. SPIE 5898). An experimental verification of a micrometeoroid impact in a dust accelerator, performed by the EPIC-pn team (MPE), demonstrated that particles of micron size could be deflected by grazing incident optics onto the focal plane of CCD (see N. Meidinger, 2002, Proc. SPIE 4851, 243-254).

The above mentioned hot column on EPIC-MOS1 CCD1 is located at RAWX=318 and is due to leaking from a defect approximately at (RAWX,RAWY)=(318,572) (in the SAS calibrated events list coordinate system) which has raised the column offset by approximately 20 ADU in imaging modes, and several tens of ADU higher in Timing mode. As a consequence, many low energy noise events are shifted above the nominal threshold. As the column passes very close to the aim point (at 3 and 9 pixels distance when EPIC-pn or RGS are prime, respectively) a significant fraction of the target source PSF is affected.

With this situation left uncorrected, events in the column are in fact flagged by the SAS task `embadpixfind` and masked out (together with the events in its neighbouring columns at either side) in the calibrated events list. Nevertheless, for imaging modes, as of Rev. 1044 the increased column noise is suppressed through a change of the on-board offset table: real events in this column, which undergo a raised baseline due the leaking hot pixels, are then restored to the correct energy through the modified offset. This allowed the column (and its neighbours) to be used for science again. However, recent measurements indicate that the column offset is evolving with time, meaning that in certain exposures the correction scheme does not restore the event energies. In these cases the events in the hot column and its neighbours will be flagged and masked through the default SAS processing.

For EPIC-MOS1 in Timing mode, the post-impact offset value is far too large to allow a meaningful correction via a modification of the on-board offset table. Nor does standard SAS processing flag or remove the hot column. Therefore, users are advised to explicitly discard the affected column and its adjacent ones from the accumulation of any scientific products; please refer to the SAS watchout web page
(`https://www.cosmos.esa.int/web/xmm-newton/sas-watchout-mos1-timing`) for a specific recipe on how to obtain a consistent set of spectral files and responses for these cases.

11 Data Analysis

This section provides an overview of the major calibration/SAS improvements in epochs corresponding to SAS version releases. Also included is a guideline of how to work with the different modes of the cameras.

11.1 New Features in SAS

11.1.1 SASv20.0

- The EPIC-to-NuSTAR empirical effective area correction can be invoked in `arfgen` (not default).[32]
- Combination of MOS and PN spectra up to 15 keV is now possible in `epicspeccombine`.[33]
- Creation of sensitivity maps in flux units.

11.1.2 SASv19.0

- A new task, `qpbselect`, has been introduced to generate quiescent particle background spectra or images from EPIC-pn FF data scaled by the number of discarded lines (a proxy for the particle background level).[34]
- A count-rate dependent photon energy correction has been implemented for EPIC-pn BURST mode data.

11.1.3 SASv18.0

- Production of a single time-stamped radiation monitor file: all radiation monitor data relevant to an observation can now be merged into a single file by the task `radmonfix`.
- Treatment of non-standard spectra: a number of warning and error messages have been added to the SAS which cope with the cases where a spectrum has been created with a non-standard pattern selection or a non-standard PI range and binning. In particular, the response matrix generation task `rmfgen` exits with an error message if it cannot produce an RMF for a particular input spectrum.
- `emldetect`: the extension likelihood, EXT_ML, is now set for all sources. An estimate of the pile-up level is made for each source and written into a new column of the output source list.
- Handling of EPIC-pn offset maps: the correct EPIC-pn offset map is now used in cases where an observation contains offset maps of multiple exposures.

11.1.4 SASv17.0

- The energy of the events recorded by the EPIC-pn camera has been shown to be dependent the background level. Tasks within the `epchain` and `epproc` processing chains have been adapted to apply an appropriate correction once the background gain dependency has been calibrated (see Sect. 2.3).

[32] `https://www.cosmos.esa.int/web/xmm-newton/sas-thread-mos-xmmselect-spectrum`
[33] `https://www.cosmos.esa.int/web/xmm-newton/sas-thread-epic-merging`
[34] `https://www.cosmos.esa.int/web/xmm-newton/sas-thread-background`

- The calculation of the size of the source extraction region for Timing/Burst mode data has been made more accurate in the `backscale` and `arfgen` tasks.
- The task `arfgen` has been generalised to allow a detector or sky coordinate image from any EPIC camera to be used to correct for bad pixels and chip gaps.
- EPIC data taken in RGS multi-pointing mode now have correct coordinate conversions applied when using `arfgen` with the `useodfatt=yes` option.
- Various updates have been made to `esas`, including making the source masks produced by the task "cheese" proportional in size to the source strength.

11.1.5 SASv16.0

- The new task `evqpb` provides a quiescent particle background events file to be associated with any given EPIC science exposure.
- The task `ebkgreg`, originally introduced for EPIC-pn, has been upgraded to work on EPIC-MOS data as well.

11.1.6 SASv15.0

- Correction of the conversion between celestial and detector coordinate systems (see Sect. 3.1).
- A new task `ebkgreg` determines the most suitable position of the background region for any source in an EPIC-pn image.
- Given a position in celestial coordinates, the new task `eupper` calculates the count rate upper limit for any EPIC sky image.
- `eboxdetect`, the task for sliding box source detection, is now compatible with detector coordinate input.
- The metatask for slew data analysis, `eslewchain`, can now produce PNG files for each subimage.

11.1.7 SASv14.0

- The `CORRAREA` empirical effective area correction can be invoked in `arfgen` (not default).
- Time-dependent EPIC-pn spectral response.
- Energy dependent EPIC-pn long-term CTI correction.
- EPIC-pn double-event energy correction.
- The rate-dependent PHA (RDPHA) correction, introduced in SASv13, is now taken as default for EPIC-pn Timing mode.
- For EPIC-pn Burst mode, the rate-dependent CTI (RDCTI) correction now takes into account the effects of X-ray loading.

11.1.8 SASv13.5

- Calibration of the contamination layer time evolution affecting the EPIC-MOS effective area.
- Improved calibration of the degradation of the EPIC-pn on-board oscillator frequency.
- Re-calibration of the energy scale in EPIC-pn Timing mode (XRL: `epreject`; RDPHA: `epevents`).

11.1.9 SASv13.0

- New operational mode in `rmfgen` to correct for moderately piled-up spectra.

11.1.10 SASv12.0

- New task `epspatialcti` to calculate a spatial-dependent gain correction in EPIC-pn.
- Improved algorithm in `arfgen` to calculate the Encircled Energy Fraction in fast modes.
- Correction to a bug in `emldetect`, which has caused in the past a 0.7" systematic position angle dependent shift in the source coordinates.
- `ELLBETA` PSF model is the default.

11.1.11 SASv11.0

- Refinement of EPIC-pn long-term CTI algorithm.
- EPIC-MOS redistribution.

11.1.12 SASv10.0

- Support of the 2-D PSF (non-default).
- EPIC spectral rebinning tool (`specgroup`).
- Flagging of uncalibrated EPIC spectral channels (`specgroup`).

11.1.13 SASv9.0

- Generation of radial profiles and comparison with the PSF model.
- Tagging of noisy EPIC-MOS CCD frames.
- EPIC spectra fluxing.

11.1.14 SASv8.0

- Improved EPIC-pn time jump detection algorithm.
- EPIC-pn rate-dependent CTI correction (default off).
- 2-D elliptical PSF parametrisation.

11.1.15 SASv7.1

- Refinement of the EPIC-MOS QE improving the cross calibration between EPIC-pn and EPIC-MOS. The EPIC-MOS cameras will return now an energy independent flux difference with respect to the EPIC-pn of ±5-7%. Before EPIC-MOS fluxes have been lower than EPIC-pn at low energies (0.2–0.8 keV) and higher at high energies (2–10 keV).

11.1.16 SASv7.0

- Column dependent CTI/Gain correction, improving line widths by up to ≃15% for some cases.
- Improved EPIC source detection and parametrisation tasks, especially related to the detection of extended sources. Robustness and efficiency have been increased, to make possible the 2XMM Catalogue derivation, which is in final preparation at the time of this release.
- Inclusion of PSF correction for EPIC timing and burst modes in response matrix generation.
- Support for arbitrary uniform binning of EPIC-MOS and EPIC-pn spectra.
- EPIC-pn FIFO reset correction corrects exposure time for saturation of the on chip amplifier stage (<5% more flux).
- EPIC-pn quadrant box temperature correction (see CAL-SRN-223).

11.1.17 SASv6.5

- `rmfgen`: The EPIC-MOS response calibration has been improved, including modelling of spatial and temporal response dependencies. This, together with calibration improvements in the newly released EPIC-pn calibration files, has as a result a much better cross-calibration among the EPIC instruments.
- EPIC source detection tasks have been upgraded to be more robust and efficient, with correct detection likelihoods.
- EPIC-MOS bad-pixel finding task has been upgraded.
- EPIC meta-tasks `emproc` and `epproc` include now all the functionalities and filtering possibilities present in the PERL scripts `emchain` and `epchain`.

11.2 Data Analysis

In the next section some general recommendations for data analysis are provided. This includes:

- Where should data be taken from the CCD.
- Which energy range should be used.
- Which pattern range should be used.
- Which response matrix should be used.
- A general caveat about "counting mode" in EPIC-pn.

For detailed guidelines on XMM-Newton data analysis please use the SAS Users' Guide at `https://xmm-tools.cosmos.esa.int/external/xmm_user_support/documentation/sas_usg/USG` and the SAS data analysis threads at `https://www.cosmos.esa.int/web/xmm-newton/sas-threads`.

11.2.1 EPIC-MOS

Imaging modes

- Source region: where appropriate.[35]
- Background region:
  - For point sources: Background can be extracted from the same observation, from another region of the same CCD, off-axis, away from source counts.
  - For extended sources: This is more complicated. Please have a look at explanatory notes available on the XMM-Newton web site at `https://www.cosmos.esa.int/web/xmm-newton/background`.

  The `ebkgreg` task, compatible with EPIC-MOS as of SASv16, can be useful in providing a suitable background region for a given source region and events image.
- Energy range: 0.2–12 keV, however, both limits depend on the aims of the analysis. In general the user should use patterns 0–12. (See XMM-Newton Users Handbook section 3.3.11 available at `https://xmm-tools.cosmos.esa.int/external/xmm_user_support/documentation/uhb/`). However, single events can be used to minimise the effects (e.g. spectral distortion) of pile-up. Single events can also be used for observations in which the best-possible spectral resolution is crucial and the corresponding loss of counts is not important. In addition the user should only use events flagged as "good" by using (`#XMMEA_EM`) in the selection expression window

[35] In the case of a high count rate point source an annular region may be useful to remove the piled-up PSF core. However, note that in order to avoid introducing systematic inaccuracies in flux, the radius of the excised core should be at least 2.5 times the instrumental pixel size (1.1" for EPIC-MOS and 4.1" for EPIC-pn). See https://www.cosmos.esa.int/web/xmm-newton/sas-thread-epatplot for details.

of `xmmselect`. When analysing spectra the user should use effective area files produced by the SAS task arfgen in conjunction with redistribution matrices produced with the SAS task `rmfgen`.

Timing mode

- Source region: where appropriate.
- Background region: background subtraction will not usually be an issue for sources observed in timing mode. However because the timing strip is only 100 pixels wide, background regions should be taken from the outer CCDs, which are collecting data in imaging mode.
- Energy range: 0.3–12 keV. Single events only for the source. Pattern 0, 1, 3 for the background region in outer CCDs. As for imaging mode, canned redistribution matrices valid for timing mode are available and should be used with ARF files produced by the SAS. Due to the large offset values following the micrometeoroid impact in Rev. 961, the column at RAWX=318 in EPIC-MOS1 Timing mode should no longer be used for science analysis. Depending on the observation, the adjacent one or two columns may be affected as well. Users are advised to remove these columns from the accumulation of any scientific products (see Sect. 10.1 for details).

11.2.2 EPIC-pn

Imaging modes

- Source region: where appropriate.[35]
- Background region:
  - For point sources: From the same observation but away from the source. Ideally the region should have the same distance to the readout node (RAWY) as the source region. This ensures that similar low-energy noise is subtracted, because this increases towards the readout-node. Do not use the columns passing through the source to avoid out-of-time events from the source, i.e. do not use an annulus around the source region. Note that since SASv6.0 it is possible to suppress the low-energy noise with the task `epreject`.
  - For extended sources: This is more complicated. Please have a look at explanatory notes available on the XMM-Newton web site at `https://www.cosmos.esa.int/web/xmm-newton/background`.

  The `ebkgreg` task, introduced for EPIC-pn in SASv15, can be useful in providing a suitable background region for a given source region and events image.
- Energy range: 0.2–12 keV For imaging purposes pattern 0-12 can in principle be used. However, since doubles (1-4), triples (5-8) and quadruples (9-12) (see XMM-Newton Users Handbook section 3.3.11 available at

https://xmm-tools.cosmos.esa.int/external/xmm_user_support/documentation/uhb/) are only created above twice, three and four times the low-energy threshold, respectively, cleanest images are produced by excluding the energy range just above the thresholds. To produce a 0.2–12 keV image one may select singles from the whole energy band and doubles only from 0.4 keV. `FLAG==0` omits parts of the detector area like border pixels, columns with higher offset, etc. This may not be desired (and is unnecessary) in the case of broadband images. For spectral analysis, response matrices are available only for singles, doubles and singles+doubles. Higher order pattern types are of low statistical significance, have degraded spectral resolution and are therefore not useful. Best spectral resolution is reached by selecting singles for the spectrum. `FLAG==0` should be used for high accuracy to exclude border pixels (and columns with higher offset) for which the pattern type and the total energy is known with significantly inferior precision. Towards higher energies, the fraction of doubles approaches that of singles and hence including doubles is recommended for increased statistics. If a sufficient number of counts are available, singles and doubles spectra can be created separately and fitted simultaneously in *XSPEC* (with all parameters including normalisations linked together). One exception is the Timing mode (see below).

To choose the valid energy band for the spectral fit it is highly recommended using the task `epatplot`. It uses as input a spatially selected (source region) event file and plots the fractions of the various patterns as function of energy. Spectral analysis should only be done in the energy band(s) where single- (and double-) fractions match the expected curves. In some observations the low-energy noise can be high, restricting the useful band at low energies. Deviations at medium energies indicate pile-up (more doubles than expected) and in such cases the inner part of the PSF in the source region should be excluded for spectral analysis. (More information on the topic of the pile-up is available in the XMM-Newton Users Handbook at `https://xmm-tools.cosmos.esa.int/external/xmm_user_support/documentation/uhb/`), Section 3.3.9).

The user should use ARF files produced by the latest version of the SAS task `arfgen` in conjunction with canned redistribution matrices (which are compatible to the CTI correction used in SASv5.3.3 or above) or produce those redistribution matrices with the SAS task `rmfgen`. For each readout mode of the EPIC-pn a set of RMF files is available (for singles, doubles, singles+doubles. Except timing mode where only singles+doubles must be used). The CTI causes a dependence of spectral resolution with distance to the readout node. Therefore the 200 lines of each CCD are divided into areas of 20 lines each (Y0 at readout, Y9 at opposite side, which includes the nominal focus point) and for each area an RMF file is available

Timing and Burst modes

- Source region: Column range centred on the source position. In the Timing and Burst modes the RAWY coordinate is related to the event time - any selection on RAWY would therefore exclude certain time periods. For Timing mode no such selection should be made and hence complete columns should be used. For Burst mode, however, a RAWY selection of RAWY<160 should be used to avoid direct illumination by the source.
- Background region: Column range covering a source-free region. For Timing mode, complete columns should be selected. For Burst mode, the identical RAWY selection as used in the source definition should be applied.

- Energy range: 0.7–12 keV
- Pattern: For Timing mode only singles+doubles (patterns 0–4) should be used. For Burst mode combinations of singles and doubles may be used as in imaging modes.

Note that detailed instructions and caveats regarding the analysis of Burst mode data can be found in Kirsch et al. 2006, A&A, 453, 173.

11.2.3 Counting Mode

If the total (source plus background) count rate is above a certain limit (a few hundred counts/s), either because of the source being too bright or due to very high flaring background, the EPIC cameras will switch to the so-called 'counting mode', a special instrument mode where no transmission of information for individual X-ray events occurs. SAS is able to correct for the dead-time yielded by the counting mode intervals. Still it is advisable to minimise as much as possible the onset of counting mode, because its loss of scientifically usable exposure time. Using a windowing mode or (for soft sources) a thicker optical blocking filter may help.

Counting mode occurs at count rates larger than 30 (700) counts per second in imaging modes (Timing mode). It affects simultaneously all CCDs in the quadrant where it occurs. In exposures taken in imaging modes it is more likely to occur at the beginning and at the end of XMM-Newton revolutions due to the higher background environment (see Fig. 15).

12 History of This Document

- Version 3.13 (29/06/2022)
  - Aligned to SASv20.0 (including 11.1)
  - Updated Sects. 2.2, 2.3
  - Fig. 8 (MOS and PN energy resolution)
  - Sect 6 and Figs. 10 and 11 (MOS and PN calibration line energy reconstruction)
  - Fig. 14 (PN absolute and relative timing)
  - Sect 10.1 (Micrometeoroid Impacts)
- Version 3.12 (23/10/2019)
  - Aligned to SASv18.0
  - Updated Sects. 2.2 and 2.3
  - Sect. 6 (allow gain shift in PN spectral analysis)
  - Fig. 8 (MOS and PN energy resolution)
  - Figs. 10 and 11 (MOS and PN calibration line energy reconstruction)
  - Sect. 8, including Fig. 14 (PN absolute and relative timing)

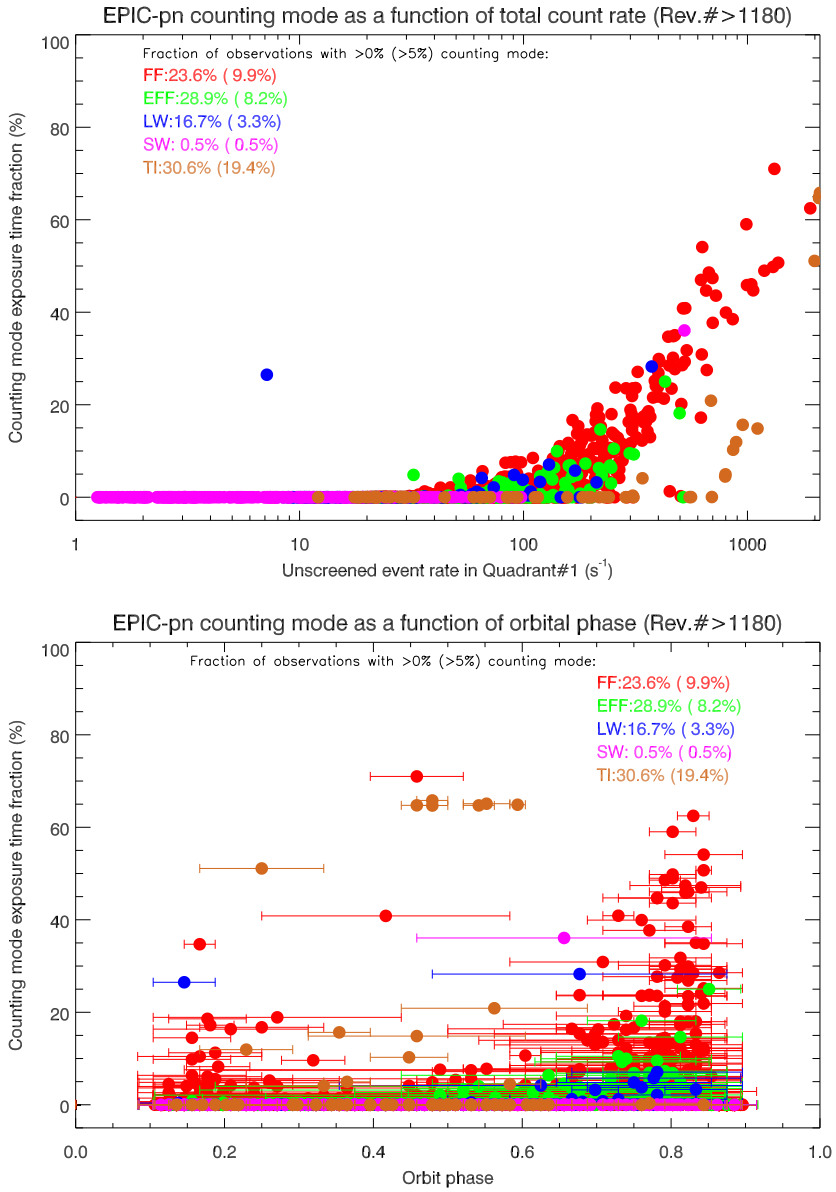

Figure 15: Fraction of exposure time affected by counting mode in EPIC-pn exposures as a function of count rate (*top panel*) and orbital phase (*bottom panel*) for all exposures from Rev. 1180 to around Rev. 1900. Instrumental modes are colour coded. The labels indicate the fraction of exposures affected by counting mode (in brackets the same number if one considers only exposures where counting mode affects a fraction of the total exposure time >5%).

- Version 3.11 (4/7/2018)
  - Aligned to SASv17.0
- Version 3.10 (28/6/2018)
  - Consistent recommended energy ranges (Sect. 11)

  - Fig. 1 (ELLBETA PSF modelling)
  - Fig. 8 (EPIC energy resolution trends)
  - Fig. 10 (MOS calibration line energy reconstruction)
  - Fig. 11 (pn calibration line energy reconstruction)

- Version 3.9 (2/1/2017)
  - Updated URL

- Version 3.8 (12/12/2016)
  - Aligned to SASv15.0 and SASv16.0
  - Added paragraph on timing accuracy in the case no TCX is available
  - Updated XMM cross-calibration summary
  - Updated micrometeoroid impact section
  - Added footnote cautioning against annular inner radii smaller than instrumental pixel size
  - Clarified TI and BU mode data analysis section, in particular that BU mode source and background regions must have identical RAWY selections
  - Fig. 8 (EPIC energy resolution trends)
  - Fig. 10 (MOS calibration line energy reconstruction)
  - Fig. 11 (pn calibration line energy reconstruction)
  - Fig. 14 (relative and absolute timing accuracy)
  - Updated URLs in view of migration to *Cosmos*

- Version 3.7 (28/08/2015)
  - Aligned to SASv14.0
  - effective area: CORRAREA
  - pn energy redistribution
  - pn CTI/gain
  - pn and MOS energy scale
  - Figs. 10 and 11 (MOS calibration line energy reconstruction)
  - Fig. 11 (pn calibration line energy reconstruction)
  - Fig. 14 (relative and absolute timing accuracy)

- Version 3.4 (26/08/2014)
  - EPIC-MOS contamination calibration
  - EPIC-pn Timing mode energy scale calibration
  - Refined calibration of the EPIC-pn on-board oscillator frequency time evolution
  - Fig. 1 (`ELLBETA` calibration accuracy)
  - Fig. 2 (relative area calibration accuracy)
  - Fig. 11 (EPIC-pn Mn K_α calibration line centroid history)

  - Fig. 14 (timing accuracy)

- Version 3.3 (2/10/2013)
  - Sect. 6 aligned to XMM-CCF-REL-300
- Version 3.2 (25/8/2013)
  - Caveat on the EPIC-pn energy reconstruction in recent exposures
  - Report on the experiment to test the accuracy of the filter transmission calibration (see Sect. 4.2)
  - Stacked residuals on 2XMM sources as a (possible) metrics of the systematic uncertainties on the effective area (see Sect. 4)
  - Update of Fig. 14 with the latest results
  - Caveat on the accuracy of timing reconstruction in EPIC-MOS (see Sect. 8)
  - MOS1-CCD3 event (see Sect. 10)
- Version 3.1 (24/7/2012)
  - Update of the Section on astrometry (including the "time-dependent boresight" implementation)
  - `ELLBETA` PSF model (see Sect. 3.2)
  - New Fig. 10, 11, and 12 (long-term calibration source centroid energy monitoring results)
  - Update of Fig. 8, and 14
- Version 3.0 (16/11/2011)
  - text streamlining and conversion into a standard LATEX XMM-Newton document
- Version 2.13 (10/6/2011)
  - Alignment to SASv11
  - Updates of Fig. 12, 14
  - New pn redistribution
  - New MOS redistribution
  - Update of the standard calibrated energy ranges for spectral fitting.
- Version 2.12 (10/1/2011):
  - New Fig.1-7 (transmission filters cross-calibration)
  - Updates of Fig. 12 using the most recent measurements
- Version 2.11 (18/07/2010)
  - Fig.1.20 (counting mode in EPIC-pn)
- Version 2.10 (24/06/2010) - Aligned to SASv10.0
  - 2-D PSF support in SASv10.0
  - EPIC-pn redistribution refinement

  - RAWY-dependent calibration of the PATTERN fraction in EPIC-pn Timing mode
  - Schedule for the implementation of a refined EPIC-pn time jumps algorithm in the SAS
  - `specgroup`
  - Update of Fig. 12 (Timing accuracy) after the regeneration of TCX files
  - Update of Fig.1-18 (cross-calibration status) to SASv9.0 results

- Version 2.9 (14/01/2010)
  - Report on the discovery of a possible underestimation of the pn resolution at $\simeq$6 keV
  - Update Fig.1-17 (Timing accuracy) with the results of the October 2009 Routine Calibration Plan measurements

- Version 2.8 (30/07/2009) - Aligned to SASv9.0
  - Update of ongoing calibration topics following the outcomes of 2009 EPIC Calibration Meeting (presentation given at this meeting are available at: `http://www.src.le.ac.uk/projects/xmm/technical/`)
  - Removal of Subsection: "Addendum: Off-axis PSF MOS speciality" of Sect. 1.1.2, now subsumed by Mateos et al. (2009, A&A, 496, 879)
  - Inclusion of figure on the stability of pn soft X-rays redistribution (now superseded)
  - Alignment of the left panel of Fig. 14 to `https://xmmweb.esac.esa.int/docs/documents/CAL-TN-0082.pdf`
  - Update of Fig.1-17 (Timing accuracy) with the results of the February 2009 Routine Calibration Plan measurements
  - SASv9.0 EPIC-related updates in Sect.2.1